ARTICLE

Evaluation of a Bead-Free Coimmunoprecipitation Technique for Identification of Virus–Host Protein Interactions Using High-Resolution Mass Spectrometry

Stacy L. DeBlasio,[1,2] Michael S. Bereman,[3] Jaclyn Mahoney,[2] Theodore W. Thannhauser,[1] Stewart M. Gray,[1,4] Michael J. MacCoss,[5] and Michelle (Cilia) Heck[1,2,4,]*

[1]U.S. Department of Agriculture, Agricultural Research Service, Emerging Pests and Pathogens Research Unit, Ithaca, New York 14853, USA; [2]Boyce Thompson Institute, Ithaca, New York 14853, USA; [3]Department of Biological Sciences, North Carolina State University, Raleigh-Durham North Carolina 27695, USA; [4]Plant Pathology and Plant-Microbe Biology Section, School of Integrative Plant Science, Cornell University, Ithaca, New York 14853, USA; and [5]Department of Genome Sciences, University of Washington, Seattle, Washington 98109, USA

Protein interactions between virus and host are essential for viral propagation and movement, as viruses lack most of the proteins required to thrive on their own. Precision methods aimed at disrupting virus–host interactions represent new approaches to disease management but require in-depth knowledge of the identity and binding specificity of host proteins within these interaction networks. Protein coimmunoprecipitation (co-IP) coupled with mass spectrometry (MS) provides a high-throughput way to characterize virus–host interactomes in a single experiment. Common co-IP methods use antibodies immobilized on agarose or magnetic beads to isolate virus–host complexes in solutions of host tissue homogenate. Although these workflows are well established, they can be fairly laborious and expensive. Therefore, we evaluated the feasibility of using antibody-coated microtiter plates coupled with MS analysis as an easy, less expensive way to identify host proteins that interact with Potato leafroll virus (PLRV), an insect-borne RNA virus that infects potatoes. With the use of the bead-free platform, we were able to detect 36 plant and 1 nonstructural viral protein significantly coimmunoprecipitating with PLRV. Two of these proteins, a 14-3-3 signal transduction protein and malate dehydrogenase 2 (mMDH2), were detected as having a weakened or lost association with a structural mutant of the virus, demonstrating that the bead-free method is sensitive enough to detect quantitative differences that can be used to pin-point domains of interaction. Collectively, our analysis shows that the bead-free platform is a low-cost alternative that can be used by core facilities and other investigators to identify plant and viral proteins interacting with virions and/or the viral structural proteins.

Key Words: potato leafroll, *Luteoviridae*, polerovirus, phloem-limited pathogen, insect-borne virus, molecular virology

INTRODUCTION

Viruses, as infectious agents, are dependent on the cells of living hosts for replication and movement. They exist as small nucleic acid structures (DNA or RNA) enclosed within a protein shell (capsid) that is sometimes surrounded by a lipid membrane or as nucleic acid-protein complexes comprised of one or more viral proteins required for movement and/or replication.[1] Once inside a host cell, these independent particles and the small repertoire of viral proteins they encode must form physical connections with various host protein complexes to evade host defenses, form viral replication sites, move cell to cell, and in some cases, manipulate host physiology to attract biotic vectors for viral dissemination.[2] Thus, identification and characterization of virus–host protein interaction networks are critical steps in understanding how pathogens cause disease. Knowledge gleaned can be useful in developing strategies aimed at disrupting these interactions to prevent infection and/or viral transmission.

Molecular-based approaches for discovering and validating protein–protein interactions include two-hybrid screening[3] and biomolecular fluorescence complementation,[4] where 2 proteins of interest (bait and prey) are genetically fused to separate fragments of a transcription factor or a fluorescent protein that are inactive in their split state. If the bait and prey physically interact, then protein-fragment complementation between the 2 halves of the transcription factor/fluorescent protein tags, respectively, leads to expression of a set of reporter genes or fluorescence

*Address correspondence to: Michelle (Cilia) Heck, U.S. Department of Agriculture, Agricultural Research Service, Emerging Pests and Pathogens Research Unit, Ithaca, New York 14853, USA (Phone: 607-254-5453; Fax: 607-254-1242; E-mail: michelle.cilia@ars.usda.gov
doi: 10.7171/jbt.17-2803-002

that can be visually assessed. Although these methods have been used successfully to identify some host proteins that directly interact with individual viral proteins,[5, 6] they are not amenable to studying interactions with multimeric protein complexes, such as assembled virion or virus replication factories. In addition, these techniques require extensive cloning and multiple rounds of screening, often in cells (*i.e.*, yeast) that are outside of the biologic context of a natural infection. Alternatively, protein co-immunoprecipitation (co-IP) works by using target protein-specific antibodies affixed to a beaded support to capture protein complexes directly from infected cells in buffer conditions that preserve biologically important protein conformations, including post-translational modifications (PTMs) that may be required for binding. Coupled to high-resolution mass spectrometry (MS), co-IP provides a high-throughput way to identify and characterize multiple virus–host interactions in a single experiment. Optimized workflows in yeast, mammals, and plants show that rapid extraction and immunoprecipitation of a protein of interest maintain the structural integrity of its associated protein complexes, while minimizing nonspecific protein interactions.[7–10] Although the technique is becoming more established in the field of virology, co-IP remains a fairly expensive and laborious process, requiring large amounts of antibody and beads, extensive optimization of conditions, and numerous tube transfers during downstream washing steps.[7, 9–11] The binding of virus-specific antibodies to microtiter plates and then the addition of diluted tissue homogenate from virus-infected plants has long been used as an effective, widely used, inexpensive method (Supplemental Table S1) to capture virus, *e.g.*, ELISA, in the field of plant virology, and may be a method to capture virus–host protein complexes that can subsequently be analyzed by MS. This technique has been used previously by Mikula *et al.*[11] to assess the interaction dynamics of human heterogeneous nuclear RNP K, a single protein, under different stress conditions using UV-C light-treated PCR plates precoated with Protein A/G.[11] This protein is a highly abundant, pleiotropic protein in human cells,[12] known to interact with other highly abundant proteins, such as ribosomal proteins.[13] Comparatively, identification of protein–protein interactions of plant viruses has its own set of challenges, in that plant cells are surrounded by thick cell walls that are recalcitrant to extraction methods used in mammalian studies.[14] In addition, most plant viruses move as multimeric structures and not as a single protein.[15] Therefore, in this study, we tested the effectiveness of using a simplified, bead-free, microplate-based co-IP assay (**Fig. 1A**), following conditions used for detection of virus by ELISA, as an alternative approach to identify plant proteins that interact with PLRV, a phloem-limited pathogen that infects solanaceous crops.

PLRV is a positive-sense, single-stranded RNA virus in the family *Luteoviridae* (genus polerovirus) that is transmitted by the green peach aphid, *Myzus persicae*, in a circulative-persistent manner.[16] Disease symptoms include severe stunting of plants, chlorosis, and leaf roll and in some potato cultivars, net necrosis, which makes tubers undesirable for sale.[17] The ~5.8 kb genome of PLRV is compact and comprised of 9 open-reading frames (ORFs) that have been found to code for biologically functional proteins.[17, 18] The capsid structure for this family is a nonenveloped, icosohedral virion composed of 2 structural proteins. The coat protein (CP), encoded by ORF3, accounts for the majority of the 180 proteins in the capsid structure. A minor capsid protein, known as the read-through protein (RTP), is generated by translational read-through of a leaky stop codon at the end of ORF3, which creates an ~500 aa carboxyl-terminal extension, known as the read-through domain (RTD). The RTP accounts for <10% of the total proteins incorporated into the capsid *via* its CP domain, with the RTD located on the surface of the capsid. It has been shown that microdomains within both the CP and RTD, as well as different nonstructural forms of these proteins, regulate virus propagation and movement through the plant and aphid[19–21] *via* specific interactions with host proteins and other nonstructural virus proteins.[10, 22, 23] Previously, we reported the identification of over 1000 plants and 3 viral proteins in complex with wild-type (WT) PLRV using a magnetic, bead-based co-IP workflow.[10, 23] Some of these viral–plant interactions were weakened or lost in the absence of the RTD (ΔRTD mutant), suggesting a role for these host proteins in viral functions regulated by this domain, *e.g.*, phloem retention, systemic movement, and symptom development.[20, 24] The 3 viral nonstructural proteins found associating with virion and/or structural proteins included the P17 movement protein (ORF4) that is required for cell-to-cell trafficking of virions,[25] the viral RNA-dependent RNA polymerase generated by a −1 ribosomal frameshift in the overlapping region of ORF1 and ORF2,[26] and the multidomain P1 protease (ORF1), which undergoes self-proteolysis to produce 3 distinct protein species, including the viral genome-linked protein.[27] The association of these nonstructural proteins in viral co-IP experiments was not dependent on the presence of the RTD.[23] With the use of the bead-free platform, we were able to identify 36 plant proteins and the P1 viral protein significantly coimmunoprecipitating with PLRV. Among the host proteins identified, 16 were also detected as high-confident interactions in our previous PLRV–plant co-immunoprecipitation analysis using antibody-coated magnetic beads.[10] Two of these host proteins were reproducibly identified as having a weakened or lost association with the ΔRTD mutant in both assays,[23] showing that the bead-free method is sensitive enough to detect quantitative differences between samples. An *in silico* functional analyses of the 36

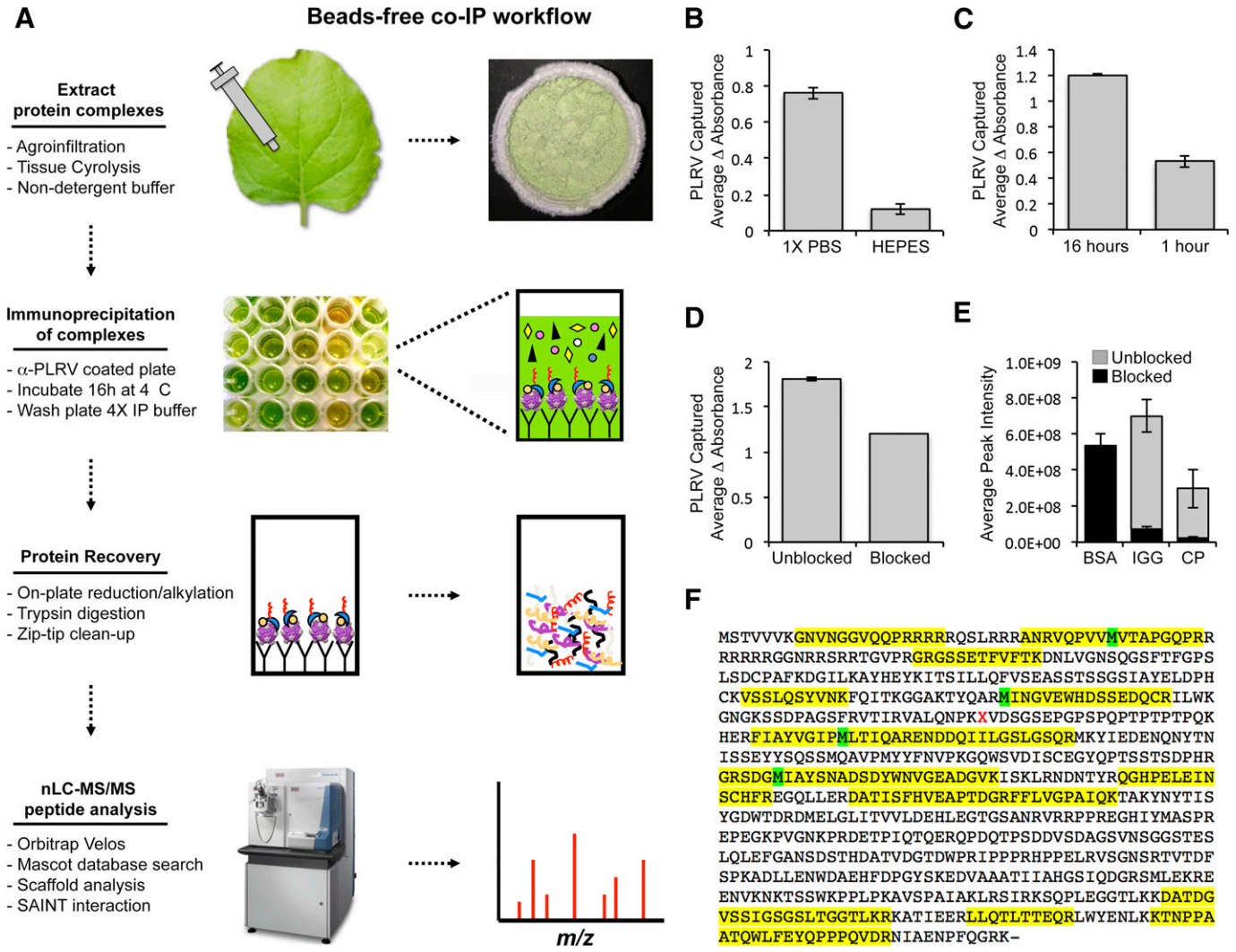

FIGURE 1

Schematic representation of the microplate-based, bead-free co-IP protocol and optimization of experimental conditions for efficient capture of PLRV–plant complexes. A) *N. benthamiana* leaves locally infected with PLRV (WT or ΔRTD) by *Agrobacterium*-mediated infiltration were cryogenically lysed using a Mixer Mill and virus–host protein complexes extracted in 1× PBS (pH 7.4) in the absence of detergent. Plant homogenate was added to a 96-well microtiter plate coated with a commercially available α-PLRV capture antibody and incubated at 4°C for ~16 h. Wells were washed and PLRV protein complexes subjected to on-plate MS sample preparation. Tryptic peptides were analyzed by nanoflow LC-MS/MS using an Orbitrap Velos mass spectrometer. Protein identification and label-free quantification of resulting peptide spectra were performed using various proteomic software tools. A detailed protocol is described in Materials and Methods. B, C) DAS-ELISA analysis of WT PLRV levels show that (B) extraction with a nondetergent-based buffer (1× PBS) and (C) a longer incubation time (16 h) result in a greater level of PLRV captured on-plate compared with conditions used for bead-based co-IP experiments,[10] *i.e.*, detergent-based HEPES buffer and a rapid 1 h incubation, respectively. D) Blocking antibody-coated microtiter plates with 3% BSA (blocked) before addition of plant homogenate resulted in slightly lower levels of captured PLRV compared with plates that were unblocked. Bar graphs represent the average change in absorbance (405 − 490 nm) ± SE, measured by DAS-ELISA for $n = 2$ biologic replicates. E) The blocking of microtiter plates with BSA (black bars) also leads to a reduction in the detection of precursor ions from IGG and PLRV CP in WT co-IP samples compared with co-IPs performed on unblocked plates (gray). Bars represent the average MS1 peak areas ± SE for 4 peptides (Supplemental Dataset S1) from BSA, IGG, and PLRV CP from WT co-IPs for $n = 9$ (blocked) and $n = 6$ (unblocked). F) Maximum amount of peptide coverage of PLRV CP/RTD in WT PLRV microtiter plate co-IPs. Yellow blocks indicated the sequence covered with peptides identified by nanoflow LC-MS/MS after analysis in Scaffold. Green blocks highlight sites where methionine was identified as oxidized.

host proteins found in complex with PLRV using the bead-free workflow revealed roles in pathways involving biosynthesis of defensive compounds, plant metabolism, and stress response.

MATERIALS AND METHODS

Plant infection

Agrobacterium tumefaciens (strain LB4404), containing infectious clones of WT PLRV,[28] or the ΔRTD mutant,[29] a PLRV that does not translate the minor capsid protein, were grown and infiltrated into individual *Nicotiana benthamiana* leaves, as outlined in DeBlasio *et al.*[10] A separate set of plants were mock infected with LB4404 as a negative control condition. Locally infected leaf tissue was harvested 3–4 d postinfiltration and stored at −80°C for subsequent experiments. Each biologic replicate consisted of a pool of 2–3 infiltrated leaves from 5 to 10 individual plants.

Lysis buffer and blocking conditions

Leaf tissue was cryogenically lysed using a Mixer Mill MM 400, following the protocol outlined in DeBlasio *et al.*[10] Protein complexes were extracted from 1 g cyro-lysed tissue on ice using 2.5 ml 1× PBS, pH 7.4, supplemented with a 1:100 dilution of Halt EDTA-free protease inhibitor (PI) cocktail (Thermo Fisher Scientific, Waltham, MA, USA) or 50 mM HEPES–KOH (pH 7.4), 0.1% Triton X-100, 110 mM potassium acetate, 2 mM $MgCl_2$, 0.5 mM PMSF, and PI (1:100) for 1 h with brief vortexing (maximum speed) every 10–15 min. The resulting homogenate was used for subsequent experiments without centrifugation.

Relative levels of WT PLRV were measured by double-antibody sandwich (DAS)-ELISA following procedures outlined in Barker and Solomon[30] and Lee *et al.*,[25] using commercially available PLRV capture and alkaline phosphatase-conjugated detection antibodies (Agdia, Elkhart, IN, USA). For the assessment of lysis buffer conditions, wells remained unblocked and were washed in the appropriate lysis buffer following our microtiter plate co-IP workflow (see below). For assessing the effect of blocking on immunocapture of PLRV, wells were washed in 1× PBS (pH 7.4) after coating with capture antibody and then blocked with 200 μl 3% bovine serum albumin (BSA) in 1× PBS (pH 7.4) for 2 h at room temperature before addition of plant homogenate (in 1× PBS, pH 7.4, plus PI). For the unblocked condition, wells were incubated with 1× PBS (pH 7.4) for 2 h. For assessment of optimal incubation time, 100 μl plant homogenate (in 1× PBS, pH 7.4, plus PI) was incubated in unblocked, antibody-coated wells for 1 or 16 h at 4°C.

For all experiments, change in absorbance (405 minus 490 nm) was measured on an Epoch spectrophotometer (BioTek Instruments, Winooski, VT, USA), 1 h after addition of phosphatase substrate (Sigma-Aldrich, St. Louis, MO, USA), dissolved in 10% diethanolamine, pH 9.8 (1 mg/ml). All values were normalized to the absorbance readings of the respective lysis buffer used.

Bead-free co-IP

One hundred microliters of polyclonal α-PLRV capture antibody (Agdia), diluted to a final concentration of 2 μg/ml in coating buffer (15 mM Na_2CO_3, 35 mM $NaHCO_3$), was added to individual wells of a 96-well microtiter plate (Agdia). This antibody has been independently validated to be specific for detecting PLRV virion and structural proteins by DAS-ELISA[19, 25] and Western blot analysis, respectively.[10, 22, 23] Plates were incubated at 37°C for 2 h. Antibody solution was removed with a pipette, and each well washed 4× with 100 μl 1× PBS, pH 7.2 (PBS), made with Nanopure H_2O, using detergent-free glassware. For the first wash, 100 μl 1× PBS was quickly pipetted up and down within the well, 4 times before being discarded. For the additional 3 washes, wells were incubated with 100 μl 1× PBS for 5 min at room temperature before the solution was discarded. The plate was dried between each washing step by inverting and tapping the plate firmly on lint-free Kimtech KimWipes (Kimberly-Clark Professional, Roswell, GA, USA). One hundred microliters of the 1× PBS-extracted plant homogenate mentioned above was added to antibody-coated wells. The plate was sealed with Parafilm M and incubated at 4°C for ~16 h in a humid chamber. Plant homogenate was carefully removed with a pipette and individual wells washed and dried following the same procedure mentioned above. Plates were stored at –80°C until the on-plate sample preparation for MS analysis. A total of 2–3 technical replicates were performed for each biologic replicate. Data represent 2 independent experiments.

Sample preparation for MS

Protein complexes resulting from the microtiter plate co-IP were reduced by adding 22 μl 6 M urea and 10 mM DTT (Sigma-Aldrich) in 100 mM ammonium bicarbonate (Sigma-Aldrich) to each well and pipetting vigorously to resuspend captured host–virus protein complexes. Plates were sealed with foil and Parafilm, sonicated for 2 min, and incubated at 37°C for 1 h. Cysteines were then blocked with 30 mM methyl methanethiosulfonate (Sigma-Aldrich) for 1 h at 37°C. Microtiter plates were sonicated for 2 min and the urea in each sample diluted to 1 M with 100 mM ammonium bicarbonate. Proteins were then digested with 100 ng sequencing grade trypsin (Promega, Madison, WI, USA) overnight at 37°C. After digestion, plates were sonicated for 10 min and dried in a vacuum concentrator. Samples were resuspended in 20 μl 0.1% formic acid, sonicated, and desalted using C18 ZipTip (MilliporeSigma,

Billerica, MA, USA), following the manufacturer's instructions. Peptides were stored at −80°C before MS analysis.

MS

For MS analysis, tryptic peptides were solubilized in 5–8 μl Solvent A by vortexing for 10 min at 37°C and bath sonication for 5 min. Splitless nanoflow chromatography was performed in the vented column configuration using a nanoACQUITY liquid chromatography (LC) system (Waters, Milford, MA, USA). Solvents A and B were 99.9/0.1 water/formic acid and 99.9/0.1 acetonitrile/formic acid, respectively. A flow rate of 2 μl/min (98% A/2% B) flushed the sample out of a 5 μl loop and onto a self-packed capillary trap column (100 μm inner diameter × 4 cm). After 10 μl wash, the 6-port valve switched and closed the vent that initiated the gradient flow (250 nl/min) and data acquisition. A 60 min analysis was run in which Solvent B ramped from 2 to 32% B over 40 min (1–41 min), held constant at 80% for 5 min (41–46 min), and initial conditions were restored for the final 14 min (46–60 min). An Orbitrap Velos (Thermo Fisher Scientific, Bremen, Germany) was operated in a data-dependent mode, where the top 10 most abundant ions were selected for tandem MS per precursor scan. For MS1 analysis performed in the Orbitrap, a scan range of a mass-to-charge ratio of 400–1400, with a resolving power of 60,000 at a mass-to-charge ratio of 400, was used. Automatic gain control was set to 1,000,000 ions, with a max ion injection time of 200 ms. For data-dependent MS2 scans, performed in the ion trap with an automatic gain control of 10,000 ions and a max ion injection time of 80 ms, a 60 s exclusion window was used to avoid repeated interrogation of abundant ions. For selection of ions, monoisotopic precursor selection was on with the exclusion of unassigned and 1^+ charge states. Each sample was analyzed once as a result of the small sample volume used to maximize peptide concentration.

MS data analysis

Protein identification and label-free quantification of MS data were performed following methods described in DeBlasio *et al.*[23] with the following exceptions: 1) oxidized methionine (variable) and methylthio on cysteines (fixed) were the only modifications used for the dataset presented, 2) a separate Mascot search (Matrix Science, London, United Kingdom) was done using lysine acetylation and phosphorylation of serine and threonine as variable modifications to identify PTMs of PLRV CP/RTD, and 3) a peptide and protein identification threshold of ≥95 and ≥90%, respectively, was used for cluster analysis in Scaffold Q+ v4.4.6 (Proteome Software, Portland, OR, USA) and the total spectral counts (SpCs) detected per biologic replicate for individual proteins reported. The false discovery rate for this analysis was <1% on the protein and peptide level. A Venn diagram presenting overlap of plant and viral proteins identified in microtiter plate immunoprecipitations was generated using VENNY 2.1 (http://bioinfogp.cnb.csic.es/tools/venny/). The interaction specificity of each prey protein with PLRV was calculated using the Significance Analysis of Interactome (SAINT) webserver,[31–33] following parameters reported in DeBlasio *et al.*[23] with WT PLRV and ΔRTD co-IPs analyzed separately against the same mock-infected control data. Contaminating mammalian proteins that were identified were dropped from further analysis. The relative levels of PLRV CP (gi|21040163), IgG1 constant region (IGG; gi|89242507), and BSA (gi|3336842) were also quantified in Skyline,[34] using precursor ion (MS1) peak integration of 3–4 peptides. MS1 and SpC data presented in Supplemental Fig. S1 were analyzed by 1-way ANOVA, followed by a Tukey's honestly significant difference *post hoc* test using the webserver http://astatsa.com/OneWay_Anova_with_TukeyHSD/. All raw MS, Mascot generic format, mzID, and Scaffold analysis files used in this study are available for download on ProteomeXchange (PXD006338). Characterization of biologic processes regulated by proteins in the identified PLRV–host interactome was performed in Blast2GO PRO 3.3.5[35] using the unique *Arabidopsis thaliana* orthologs of *N. benthamiana* proteins found to form confident interactions [probability score (SP) ≥ 0.6] with PLRV. Putative biologic functions of featured proteins for **Table 1** were manually curated from our in-house database or through literature searches.

RESULTS AND DISCUSSION

Bead-free co-IP workflow

For immunocapture of PLRV–plant protein complexes on microtiter plates, we compared methods commonly used for detection of PLRV by DAS-ELISA,[19, 25] an immunocapture-based technique used for plant infection diagnostics,[30] with those previously determined to be optimal for capture of PLRV–plant protein complexes using antibody-coated magnetic beads.[10, 23] Plates were coated with a commercially available pAb, specific for detecting PLRV virion and the nonincorporated forms of both structural proteins, including the truncated and multimeric forms of the RTP that have been described previously.[10, 19, 22, 23, 25, 36] In our bead-based workflow, cellular lysis in a detergent-based HEPES buffer, supplemented with PIs, resulted in higher levels of PLRV extracted from cryo-milled *N. benthamiana* tissue that did not interfere with enrichment of virus on antibody-coated magnetic beads.[10] However, use of this buffer composition resulted in a severe reduction (6.3-fold) in the amount of PLRV captured on antibody-coated microtiter wells compared with solubilization/washing in 1× PBS (pH 7.4), supplemented with PIs, the buffer typically used for detection

TABLE 1

Host and viral proteins found significantly enriched in PLRV co-IPs using the beads-free method

Accession number[c]	Protein symbol[d]	Biologic function[e]	Fold enrichment bead-free co-IP[a]			SAINT probability[b]		
			WT/mock	ΔRTD/mock	WT/ΔRTD	WT PLRV	ΔRTD	Magnetic beads[f]
gi|9629162	P1	PLRV replication	±	±	0.1	0.13	0.61	WT = ΔRTD
NbS00007737g0010.1	GRF2	Plant signal transduction	±	nd	±	0.71	nd	WT > ΔRTD
NbS00053961g0017.1	LOX1	Defense response	±	±	1.0	1	0.98	nd
NbS00041882g0003.1	HS17C	Protein folding	±	±	0.5	0.75	0.66	nd
NbS00025860g0007.1	HSP12	Protein folding	±	±	0.5	0.74	0.66	WT = ΔRTD
NbC23171932g0001.1	RABE1b	Translation	±	±	1.0	0.71	0.65	WT = ΔRTD
NbS00014538g0012.1	ASD	Amino acid biosynthesis	±	±	0.9	0.71	0.62	nd
NbS00023487g0001.1	TPS21	Terpinoid biosynthesis	±	±	1.0	0.68	0.66	nd
NbS00050323g0002.1	FBA	Calvin cycle	±	±	0.6	0.63	0.64	WT = ΔRTD
NbS00004447g0101.1	–	Unknown	±	±	0.6	0.61	0.66	nd
NbS00012575g0015.1	MDH	Plant defense	±	±	0.7	0.59	0.65	WT > ΔRTD
NbS00027674g0005.1	ATHSP22.0	Protein folding	±	±	0.6	0.49	0.99	nd
NbS00007018g0006.1	HSP17.6II	Protein folding	±	±	0.4	0.39	0.66	nd
NbS00001020g0016.1	CLPR1	Protein degradation	±	±	0.3	0.22	0.62	nd
NbS00009873g0002.1	NAGK	Amino acid biosynthesis	±	±	0.3	0.22	0.61	nd
NbS00004083g0015.1	TCPZ	Protein folding	±	±	0.1	0.13	0.81	nd
NbS00003113g0010.1	MOD1	Fatty acid biosynthesis	±	±	0.1	0.13	0.61	nd
NbS00001709g0013.1	mMDH2	Response to phosphorus	14.3	7.0	2.0	0.96	0.57	WT > ΔRTD
NbS00016355g0001.1	FDH	Respiration	9.4	9.5	1.0	0.71	0.63	nd
NbS00043069g0004.1	PCAP1	Abiotic stress protein	8.5	7.3	1.2	0.89	0.66	nd
NbS00015135g0014.1	MVA1	Isoprenoid biosynthesis	6.0	6.5	0.9	0.7	0.93	WT = ΔRTD
NbS00045109g0006.1 (+1)	OMT1	Lignin biosynthesis	5.0	7.7	0.7	0.72	0.9	nd
NbS00024018g0015.1	CCT2	Protein folding	4.5	9.0	0.5	0.41	0.91	WT > ΔRTD
NbS00045171g0004.1	FBA2	Citric acid cycle	3.8	4.2	0.9	0.74	0.88	WT = ΔRTD
NbS00011007g0119.1	–	Unknown	3.6	3.0	1.2	0.64	0.59	WT > ΔRTD
NbS00043465g0007.1 (+2)	PKT3	Fatty acid biosynthesis	3.4	10.0	0.3	0.34	0.78	nd
NbS00033090g0004.1	RPS4.1	Protein translation	3.3	0.5	7.2	0.73	0.07	WT = ΔRTD
NbS00012742g0007.1	VLN2	Actin-binding protein	2.6	5.3	0.5	0.41	0.65	WT > ΔRTD
NbS00021865g0002.1 (+2)	6PGD2	Pentose phosphate pathway	2.4	5.4	0.4	0.24	0.65	WT > ΔRTD
NbS00040865g0006.1	BIP1	Protein folding	2.4	2.7	0.9	0.47	0.84	WT = ΔRTD
NbS00023365g0001.1	VHA-D	Vacoule homeostastis	1.3	2.9	0.5	0.25	0.62	WT > ΔRTD
NbS00010935g0008.1	RGP3	Plasmodesmata regulation	1.0	2.3	0.4	0.24	0.68	WT > ΔRTD

[a]Fold enrichment calculation based on the ratio of average total SpCs detected in PLRV microtiter plate co-IPs to mock-infected controls and to each other. ±, Proteins found in 1 co-IP versus another. nd, Protein not detected.
[b]SAINT SP indicating interaction confidence.
[c]Protein identifier corresponding to protein sequences found in our in-house protein database (http://bti.cornell.edu/nicotiana-benthamiana/). Parenthesis indicates the number of additional protein family members identified as forming high-confident interactions with PLRV (Supplemental Dataset S3).
[d]Protein symbols manually curated from our in-house database. −, Proteins in the database without symbols.
[e]Putative biologic function based on what is known for corresponding orthologous protein in *A. thaliana*.
[f]Interaction category based on the detection of these proteins as enriched equally in PLRV co-IPs compared with mock (WT = ΔRTD) or enriched in WT PLRV co-IPs compared with ΔRTD (WT > ΔRTD) using antibody-coated Protein A Dynabeads.[10, 18] nd, Protein not detected in the bead-based co-IP experiment comparing WT PLRV with ΔRTD.[18]

of PLRV by DAS-ELISA[25] (Fig. 1B). Likewise, the reduction of the incubation time of PLRV-infected homogenate with antibody-coated wells from ~16 h (used for DAS-ELISA) to 1 h (used for bead-based methods) also resulted in a lower amount (2.2-fold) of captured PLRV (Fig. 1C). Next, we tested whether the blocking of the microtiter wells would increase the interaction specificity of PLRV with antibody. This method is often implemented in diagnostic protocols to increase signal-to-noise by preventing nonspecific reactants from binding to the microtiter well.[37] In our study, the blocking of antibody-coated plates with 3% BSA before the addition of infected plant homogenate led to a slight decrease in the amount of PLRV captured (Fig. 1D). More importantly, the large abundance of BSA drastically lowered our ability to detect peptides from IGG and PLRV CP in WT co-IP samples by data-dependent MS compared with co-IP experiments performed on unblocked plates (Fig. 1E). Detection of lower abundant peptides in complex samples, such as co-IP mixtures, becomes difficult as a result of the dynamic range of coeluting peptides from abundant proteins competing for MS/MS acquisition.[38]

Collectively, our results show that optimal conditions for immunoprecipitation of PLRV using antibody-coated microtiter plates are in line with what is best for detection of virus using ELISA rather than conditions used for bead-based immunoprecipitation of virus-plant complexes, with the exception of blocking plates with BSA. It is possible that in the bead-free system, the use of detergent interferes with binding of virus to antibody. Alternatively, the adherence of antibody to the microtiter plate matrix may be weaker than in the bead-based system, where antibody is either covalently conjugated to magnetic beads in a uniform manner[9] or tightly bound by Protein A.[10] Thus, the washing of wells with detergent would readily disrupt retention of the antibody. A cost analysis of the microtiter plate assay compared with our previous bead-based assay (Supplemental Table S1) revealed a $59 decrease in spending on matrix support, over $200 saved in purchasing a commercially available α-PLRV antibody optimized for DAS-ELISA compared with using a custom-made antibody that required user validation of specificity and cross-absorption before use with magnetic beads,[14] and the use of nanograms instead of micrograms of trypsin. Money was also saved on reagents and materials not required for the bead-free workflow, such as the protein LoBind microfuge tubes, a magnet, and Pmax Surfactant for trypsin digestion. Although the overall time spent completing the bead-free workflow was longer (>24 h) compared with using magnetic beads (~6 h, depending on the number of samples), time spent actively manipulating co-IP samples was longer for the bead-based method as a result of the individual washing steps, which are more amenable to high-throughput automation when using a microtiter plate.

Mass spectrometric analysis of plant–virus complexes captured using bead-free co-IP platform

With the use of our bead-free co-IP workflow (Fig. 1A), we detected peptides spanning the entire PLRV RTP in WT PLRV microtiter plate co-IPs with sequence coverage between 1 and 46% (Fig. 1F). This result is similar to what we observed when using antibody-coated magnetic beads to capture PLRV–host complexes.[10] The PLRV RTP was detected with an average Mascot protein score of 743 and an average exponentially modified protein abundant index of 1.8 in WT co-IP samples. These scores were lower than what we observed when using antibody-coated magnetic beads (13,632 and 78.23, respectively),[10] indicating a lower abundance of PLRV captured using the bead-free method. As expected, peptides from the RTD were not detected in ΔRTD mutant co-IP experiments (data not shown). Previous studies with mammalian cells have shown that the use of a similar bead-free immunoprecipitation technique coupled to offline separation of captured proteins by SDS-PAGE before MS analysis allowed for the identification of bait peptides containing PTMs, including phosphorylation and acetylation.[11] Despite the identification of 3 phosphorylated peptide isoforms from the PLRV RTD in our bead-based study, which did not include SDS-PAGE separation of proteins complexes,[10] these were not identified here.

Levels of PLRV, captured per well, were too low to detect by conventional assays, such as Western blot analysis and Bradford assay, after sample incubation (data not shown). Therefore, reproducibility of well-to-well protein recovery was assessed by quantifying the number of total SpCs and the MS1 peptide intensities detected for IgG and the PLRV structural proteins across all technical replicates using the proteomic software tools Scaffold Q+ and Skyline,[34] respectively. On average, levels of IgG were not significantly different among WT PLRV, ΔRTD, and mock-infected co-IP samples by SpC or MS1 peak integration (Supplemental Fig. S1A, B), indicating good reproducibility of antibody coating. However, we observed a 30.2% coefficient of variation (CV) of SpC and a median CV of 60.7% for MS1 peak intensities among co-IP technical replicates (Supplemental Dataset S2), suggesting that well-to-well protein recovery was variable. Interestingly, median levels of PLRV CP in mutant co-IPs were 1.7 (SpC) and 2.5 (MS1 of 3 CP peptides)-fold lower compared with WT (Supplemental Fig. S1C, D), a difference we did not observe when using magnetic beads.[23] However, statistical analysis (ANOVA, Tukey's honestly significant difference) indicated these differences as being insignificant ($P > 0.07$). As the antibody used in the analysis was a pAb, raised against sucrose density-purified virion, it is possible that the mutant virion is captured less efficiently as a result of the loss of epitopes from the RTD,

which would lead to lower levels of CP being detected in mutant co-IP samples. CV values for CP MS1 signal intensities for ΔRTD and WT technical replicates were 44.4 and 105.9%, respectively. CV for SpC was 22.6 and 79.6% for ΔRTD and WT, respectively. As a result of the well-to-well variability we observed, SpC data generated from technical replicates for each prey protein were combined into a single biologic replicate for subsequent analyses to identify PLRV interacting partners.

In total, 849 *N. benthamiana* and 2 PLRV nonstructural proteins (P1 and P17) were detected in microtiter plate co-IP experiments (Supplemental Dataset S3). **Figure 2A** shows a Venn diagram presenting the number of prey proteins detected in each of the co-IP PLRV infection conditions and their overlap. The majority of prey proteins detected (467) were shared among all PLRV co-IP conditions, including negative controls, 25 of which had an average SpC that was ≥2-fold enriched in PLRV (WT and ΔRTD) co-IPs compared with mock-infected, negative controls (Fig. 2B and Supplemental Dataset S3). Eighty-one and 51 proteins were detected in WT or mutant PLRV samples only, whereas 64 proteins were detected in both PLRV co-IPs but not mock-infected negative controls, including the 2 nonstructural viral proteins P1 and P17 (Supplemental Dataset S3). An additional 188 plant proteins were detected in either mock-infected-only or mock-infected and 1 of the PLRV co-IP conditions, with only 16 of these proteins enriched ≥2-fold in the PLRV bead-free co-IPs (WT or ΔRTD) compared with mock. The comparison of all proteins identified in our microtiter plate dataset with those identified as forming high-confident interactions with WT PLRV using antibody-coated magnetic beads[10, 23] revealed that proteins enriched ≥2-fold in both WT and ΔRTD plate co-IPs compared with mock-infected controls exhibited the highest degree of overlap (64%) with proteins identified as interacting with PLRV in the bead-based assay, whereas proteins that were detected in both our viral bead-free co-IPs but not detected in mock-infected controls shared only a 40.6% overlap in identity (Fig. 2 and Supplemental Dataset S3). Those proteins detected in only 1 of the viral bead-free co-IPs but not mock-infected controls also showed a high degree of overlap (53–57%) with proteins identified within the bead-based plant–PLRV interactome, whereas proteins detected in either mock-infected-only or mock-infected and the WT PLRV co-IPs had the lowest percentage of overlap (Fig. 2A). Surprisingly, out of 408 plant proteins that were not enriched (<2-fold) in viral bead-free co-IPs compared with the negative controls, we found that ~62% of these proteins were significantly enriched using the magnetic bead approach (Supplemental Dataset S3). It is

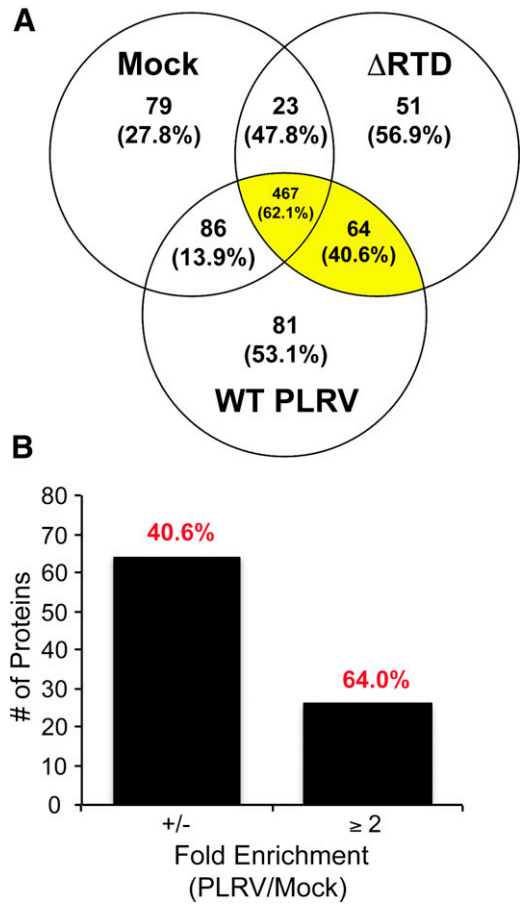

FIGURE 2

co-IP of PLRV from infected tissue using antibody-coated microtiter plates enriches for host–virus interactions that overlap with those identified using a bead-based protocol. A) Venn diagram shows the number of plant and viral proteins identified by at least 1 unique peptide spectra in microtiter plate co-IPs from plants infected with WT PLRV (n = 4 biologic, 13 technical replicates) or the ΔRTD mutant (n = 3 biologic, 9 technical replicates) compared with negative control immunoprecipitations from mock-infiltrated tissue (n = 3 biologic, 10 technical replicates). Protein annotations and total SpC data for these proteins can be found in Supplemental Dataset S3. For each category, the percent overlap in identity with proteins detected as significantly enriched in WT PLRV co-IPs using antibody-coated magnetic beads[10, 18] is shown in parentheses. Proteins found enriched in co-IPs from both WT PLRV- and ΔRTD-infected tissue compared with mock-infected co-IPs (categories highlighted in yellow) were identified as forming high-confident interactions by SAINT[24–26] (Table 1). B) Number of plant/viral proteins identified as enriched ≥2-fold in both WT PLRV and ΔRTD microtiter plate co-IPs compared with mock-infected controls. Fold change was computed as the ratio of average total SpCs assigned in PLRV co-IPs compared with mock using Scaffold. The number of host proteins that were detected in the PLRV co-IPs by SpC but not in mock is indicated by ±. The percent overlap with proteins identified as significantly enriched in WT PLRV co-IPs using antibody-coated magnetic beads[10, 18] compared with negative controls is shown in red.

interesting to note that most of these plant proteins were abundantly detected (average SpC >20) in our co-IP samples, suggesting that there may be a limit in detecting plant–virus interactions using the bead-free workflow when the prey protein is highly abundant within the homogenate. Alternatively, further optimization of antibody concentration and/or antigen affinity could lead to an increase in the capture of lower abundant or transient host–virus complexes, as has been reported for bead-based co-IPs.[9] Furthermore, differences in lysis buffer conditions between the two methodologies may also be a contributing factor.

To assign confidence scores to the enriched interactions detected in our dataset, we used SAINT, a proteomic software tool that statistically models protein SpCs to calculate interaction SPs based on fold enrichment and reproducible detection of peptides in biologic replicates of bait co-IPs compared with negative controls.[31, 32] From our current dataset, we detected a total of 36 *N. benthamiana* proteins and 1 nonstructural viral protein (P1 protein) having SPs indicative of confident interaction with PLRV (SP ≥0.6) in at least 1 of the viral co-IPs (Table 1), 50% of which were also identified as significantly interacting with PLRV in our magnetic bead-based method (Supplemental Dataset S3). One of these proteins—luminal binding protein—was previously identified by our group as directly interacting with PLRV CP to regulate functionally PLRV accumulation *in planta* using protein interaction reporter, an approach that uses chemical cross-linking and high-resolution MS to define interaction topologies.[22] The remaining 18 proteins detected as significantly coimmunoprecipitating with PLRV (Table 1) were unique to the bead-free method, most likely as a result of the differences in lysis buffers used and/or immunoprecipitation times between the two co-IP methods. All proteins found to be forming high-confidence interactions (SP ≥0.6) in the bead-free assay, except one—general regulatory factor 2 (GRF2)—were enriched in both WT PLRV and ΔRTD compared with mock-infected controls, indicating that these are proteins whose interaction with PLRV is dependent on the CP. Three proteins—GRF2, mMDH2, and 40S ribosomal protein S4 (RPS4.1)—exhibited a lost or weakened association in ΔRTD plate co-IPs compared with WT, suggesting an interaction dependence on the RTD domain. However, only GRF2 (14-3-3 signal transduction molecule[39]) and mMDH2 were identified as having the same interaction dynamics in our magnetic bead-based experiments (Table 1). RPS4.1 was identified as interacting equally with WT and mutant when antibody-coated magnetic beads were used.[23] Conversely, some proteins that were identified as having lost or weakened association with ΔRTD in our magnetic bead co-IPs[23] were not detected as such in the bead-free platform (Table 1 and Supplemental Dataset S3). Proteins that were only detected in either WT PLRV or ΔRTD microtiter plate co-IPs, compared with mock-infected samples (±, Table 1 and Supplemental Dataset S3), had some of the lowest confidence interactions scores as a result of inconsistent detection across biologic replicates, despite >53% of these proteins being detected as significantly enriched with WT PLRV in the magnetic bead-based method (Fig. 2A).[10, 23] Together, our analysis shows that the bead-free microtiter plate platform can be used to identify confidently some plant and viral proteins interacting with virion and/or the structural proteins, although not all viral–host interactions may be stable or abundant enough for the quantification of these differences using 3–4 biologic replicates, as they can be using magnetic beads. Whereas not mutually exclusive, an increased level of nonspecific interactions occurring in antibody-coated microtiter wells could have also contributed to the variability of protein complex stability that we observed in the bead-free co-IPs compared with the magnetic bead-based workflow, which is optimized for rapid immunoprecipitation to minimize such interactions.[7, 9]

In silico characterization of the bead-free PLRV–plant interactome

To characterize the function of *N. benthamiana* proteins identified in our bead-free co-IP study, we used an homology-based bioinformatics approach to identify gene ontology terms associated with the *A. thaliana* orthologs of host proteins that we found significantly enriched in PLRV co-IP experiments (Table 1). Sequence annotation, statistics, and visualization of enriched biologic processes in our current PLRV–host interaction dataset were performed in Blast2GO PRO.[35] Interestingly, processes associated with plant metabolism, stress response, and small molecule biosynthesis were those terms associated with the greatest number of host proteins in the network (**Fig. 3**). Lipoxygenase 1 (LOX1) was a host protein that had the highest SAINT interaction scores in both the WT and mutant PLRV co-IPs (SP ≥0.98; Table 1), indicating it as a high-confident interacting partner of virus. This specific protein was not identified in our pervious interactome study using magnetic beads, although other LOX family members were.[10] LOXs are enzymes that catalyze the hydroperoxidation of polyunsaturated fats for the synthesis of many bioregulatory molecules, including the defense response hormone jasmonic acid.[40] Several LOXs, including LOX1, have been implicated in the mediation of plant immunity in response to pathogen and insect attack, specifically through the production of volatile substances.[41, 42] We also identified vetispiradiene synthase [terpene synthase 21 (TPS21)] and caffeic acid 3-*O*-methyltransferase 1

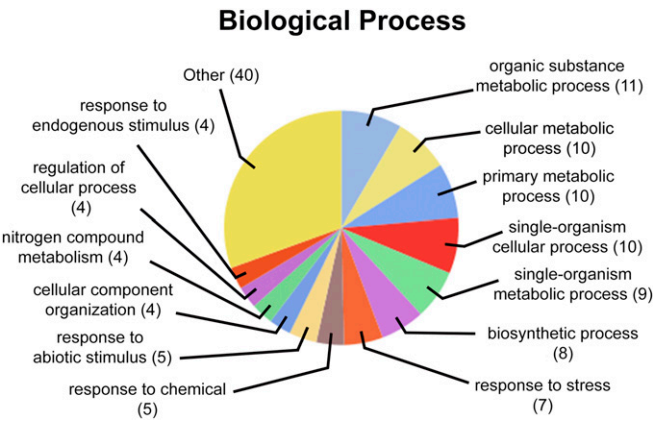

FIGURE 3

Gene ontology analysis of biologic processes regulated by *N. benthamiana* proteins identified in complex with PLRV in the bead-free co-IP dataset. The unique *A. thaliana* orthologs of *N. benthamiana* proteins found to form confident interactions (SP ≥0.6, Table 1) with virus were analyzed for associated biologic processes using Blast2GO[28] and visualized at a tree level of 3. The number of proteins associated with a term is given in parenthesis. Proteins with terms that made up <4% of the total were grouped as "other."

(OMT1), additional enzymes involved in the biosynthesis of defensive molecules, in response to pathogen infection.[43, 44] OMT1 plays a central role in the biosynthesis of lignin,[45] a polymer that is important for maintaining cell-wall integrity during pathogen resistance.[46] In fact, protein expression of OMT has been found to be up-regulated in maize infected with rice black-streaked dwarf virus,[47] a double-stranded RNA virus from the family *Reoviridae*. TPS21, also known as α-humulene/(−)-(E)-β-caryophyllene synthase, is responsible for the formation of almost all sesquiterpenes emitted from *Arabidopsis* flowers.[48] It is known that infection of potato plants with PLRV influences the behavior of its aphid vector, *M. persicae*, through the induction of plant volatiles that attract and induce feeding, which promotes virus acquisition and ultimately transmission.[49] α-Humulene was 1 of 6 headspace volatiles elevated by PLRV infection but not infection by potato virus Y and X,[49] a group of plant viruses that are mechanically transmitted and do not require prolonged feeding of insect vectors for transmission.[50] Our data suggest that PLRV may manipulate plant physiology by interacting with and changing the activity of key enzymes in pathways that lead to the biosynthesis of volatiles and compounds that are attractive to aphids to facilitate its own transmission. These pathways also play a role in plant defense,[41, 43, 44] which PLRV would need to sequester to mount a successful infection. Future work on disrupting these plant–virus interactions would provide further insight to the function of these host proteins in the PLRV disease cycle and may lead to novel strategies for control of *Luteoviridae* infection of crop plants.

CONCLUSIONS

Comparison of plant and viral proteins identified as interacting directly or indirectly with PLRV using a bead-free immunoprecipitation platform with those identified using a traditional bead-based method that is more comprehensive and also more costly revealed that some plant–virus protein interactions can be reproducibly identified using the less-expensive assay. Our work provides core labs aiming to reduce costs and those looking to do a cursory screen for binding partners with an easier, higher throughput alternative to characterizing interactions between host and viral proteins.

ACKNOWLEDGMENTS

The authors thank Tom Hammond (Cornell University) for care of plants, Tara Fish [U.S. Department of Agriculture (USDA), Agricultural Research Service] for guidance on MS sample preparation, Kevin Howe for help with ProteomeXchange, James VanEe and John Flaherty at Cornell University's Institute for Biotechnology Bio-IT Facility for information technology support, Dr. Greg Martin (Boyce Thompson Institute) for access to the *N. benthamiana* genome sequencing data before publication, and Richard Johnson (University of Washington) for his help with data archiving issues. Funding was provided by USDA National Institute of Food and Agriculture Grant 1907-22000-021-20, National Science Foundation Grant 1354309, and USDA Current Research Information System Project Numbers 8062-22000-022-00-D and 8062-22410-006-00-D. The authors declare no conflicts of interest.

REFERENCES

1. Rossmann MG. Structure of viruses: a short history. *Q Rev Biophys* 2013;46:133–180.
2. Zaitlin M, Hull R. Plant virus-host interactions. *Annu Rev Plant Physiol* 1987;38:291–315.
3. Brückner A, Polge C, Lentze N, Auerbach D, Schlattner U. Yeast two-hybrid, a powerful tool for systems biology. *Int J Mol Sci* 2009;10:2763–2788.
4. Bhat RA, Lahaye T, Panstruga R. The visible touch: *in planta* visualization of protein-protein interactions by fluorophore-based methods. *Plant Methods* 2006;2:12.
5. Pfefferle S, Schöpf J, Kögl M, et al. The SARS-coronavirus-host interactome: identification of cyclophilins as target for pan-coronavirus inhibitors. *PLoS Pathog* 2011;7:e1002331.
6. Rodriguez-Medina C, Boissinot S, Chapuis S, et al. A protein kinase binds the C-terminal domain of the readthrough protein of *Turnip yellows virus* and regulates virus accumulation. *Virology* 2015;486:44–53.
7. Conlon FL, Miteva Y, Kaltenbrun E, Waldron L, Greco TM, Cristea IM. Immunoisolation of protein complexes from *Xenopus*. *Methods Mol Biol* 2012;917:369–390.
8. Cristea IM, Carroll JW, Rout MP, Rice CM, Chait BT, MacDonald MR. Tracking and elucidating alphavirus-host protein interactions. *J Biol Chem* 2006;281:30269–30278.
9. Cristea IM, Williams R, Chait BT, Rout MP. Fluorescent proteins as proteomic probes. *Mol Cell Proteomics* 2005;4:1933–1941.
10. DeBlasio SL, Johnson R, Mahoney J, et al. Insights into the polerovirus-plant interactome revealed by coimmunoprecipitation and mass spectrometry. *Mol Plant Microbe Interact* 2015;28:467–481.
11. Mikula M, Rubel T, Karczmarski J, Statkiewicz M, Bomsztyk K, Ostrowski J. Beads-free protein immunoprecipitation for a

mass spectrometry-based interactome and posttranslational modifications analysis. *Proteome Sci* 2015;13:23.
12. Chaudhury A, Chander P, Howe PH. Heterogeneous nuclear ribonucleoproteins (hnRNPs) in cellular processes: focus on hnRNP E1's multifunctional regulatory roles. *RNA* 2010;16:1449–1462.
13. Mikula M, Dzwonek A, Karczmarski J, et al. Landscape of the hnRNP K protein-protein interactome. *Proteomics* 2006;6: 2395–2406.
14. Stewart LR, Ding B, Falk BW. Viroids and phloem-limited viruses: unique molecular probes of phloem biology. In Thompson GA, van Bel AJ. (eds): *Phloem: Molecular Cell Biology, Systemic Communication, Biotic Interactions*. Hoboken, NJ: John Wiley and Sons, 2013:271–292.
15. Hipper C, Brault V, Ziegler-Graff V, Revers F. Viral and cellular factors involved in Phloem transport of plant viruses. *Front Plant Sci*. 2013;4:154.
16. Gray S, Cilia M, Ghanim M. Circulative, "nonpropagative" virus transmission: an orchestra of virus-, insect-, and plant-derived instruments. *Adv Virus Res* 2014;89:141–199.
17. Taliansky M, Mayo MA, Barker H. *Potato leafroll virus*: a classic pathogen shows some new tricks. *Mol Plant Pathol* 2003;4:81–89.
18. Smirnova E, Firth AE, Miller WA, et al. Discovery of a small non-AUG-initiated ORF in poleroviruses and luteoviruses that is required for long-distance movement. *PLoS Pathog* 2015;11:e1004868.
19. Lee L, Kaplan IB, Ripoll DR, Liang D, Palukaitis P, Gray SM. A surface loop of the potato leafroll virus coat protein is involved in virion assembly, systemic movement, and aphid transmission. *J Virol* 2005;79:1207–1214.
20. Peter KA, Gildow F, Palukaitis P, Gray SM. The C terminus of the polerovirus p5 readthrough domain limits virus infection to the phloem. *J Virol* 2009;83:5419–5429.
21. Peter KA, Liang D, Palukaitis P, Gray SM. Small deletions in the potato leafroll virus readthrough protein affect particle morphology, aphid transmission, virus movement and accumulation. *J Gen Virol* 2008;89:2037–2045.
22. DeBlasio SL, Chavez JD, Alexander MM, et al. Visualization of host-polerovirus interaction topologies using protein interaction reporter technology. *J Virol* 2015;90:1973–1987.
23. DeBlasio SL, Johnson R, Sweeney MM, et al. Potato leafroll virus structural proteins manipulate overlapping, yet distinct protein interaction networks during infection. *Proteomics* 2015; 15:2098–2112.
24. Boissinot S, Erdinger M, Monsion B, Ziegler-Graff V, Brault V. Both structural and non-structural forms of the readthrough protein of cucurbit aphid-borne yellows virus are essential for efficient systemic infection of plants. *PLoS One* 2014;9:e93448.
25. Lee L, Palukaitis P, Gray SM. Host-dependent requirement for the *Potato leafroll virus* 17-kda protein in virus movement. *Mol Plant Microbe Interact* 2002;15:1086–1094.
26. Kujawa AB, Drugeon G, Hulanicka D, Haenni AL. Structural requirements for efficient translational frameshifting in the synthesis of the putative viral RNA-dependent RNA polymerase of potato leafroll virus. *Nucleic Acids Res* 1993;21:2165–2171.
27. Li X, Halpin C, Ryan MD. A novel cleavage site within the potato leafroll virus P1 polyprotein. *J Gen Virol* 2007;88:1620–1623.
28. Franco-Lara LF, McGeachy KD, Commandeur U, Martin RR, Mayo MA, Barker H. Transformation of tobacco and potato with cDNA encoding the full-length genome of *potato leafroll virus*: evidence for a novel virus distribution and host effects on virus multiplication. *J Gen Virol* 1999;80:2813–2822.
29. Liang D, Gray SM, Kaplan I, Palukaitis P. Site-directed mutagenesis and generation of chimeric viruses by homologous recombination in yeast to facilitate analysis of plant-virus interactions. *Mol Plant Microbe Interact* 2004;17:571–576.
30. Barker H, Solomon RM. Evidence of simple genetic control in potato of ability to restrict potato leaf roll virus concentration in leaves. *Theor Appl Genet* 1990;80:188–192.
31. Choi H, Larsen B, Lin ZY, et al. SAINT: probabilistic scoring of affinity purification-mass spectrometry data. *Nat Methods* 2011;8:70–73.
32. Choi H, Liu G, Mellacheruvu D, Tyers M, Gingras AC, Nesvizhskii AI. Analyzing protein–protein interactions from affinity purification-mass spectrometry data with SAINT. *Curr Protoc Bioinformatics* 2012:39:8.15.1–8.15.23.
33. Mellacheruvu D, Wright Z, Couzens AL, et al. The CRAPome: a contaminant repository for affinity purification-mass spectrometry data. *Nat Methods* 2013;10:730–736.
34. MacLean B, Tomazela DM, Shulman N, et al. Skyline: an open source document editor for creating and analyzing targeted proteomics experiments. *Bioinformatics* 2010;26:966–968.
35. Conesa A, Götz S, García-Gómez JM, Terol J, Talón M, Robles M. Blast2GO: a universal tool for annotation, visualization and analysis in functional genomics research. *Bioinformatics* 2005;21:3674–3676.
36. DeBlasio SL, Johnson RS, MacCoss MJ, Gray SM, Cilia M. Model system-guided protein interaction mapping for virus isolated from phloem tissue. *J Proteome Res* 2016;15:4601–4611.
37. Xiao Y, Isaacs SN. Enzyme-linked immunosorbent assay (ELISA) and blocking with bovine serum albumin (BSA)–not all BSAs are alike. *J Immunol Methods* 2012;384:148–151.
38. Yeom J, Kabir MH, Lee C. Impact of data-dependent exclusion list based mass spectrometry on label-free proteomic quantification. *Rapid Commun Mass Spectrom* 2015;29:128–134.
39. DeLille JM, Sehnke PC, Ferl RJ. The arabidopsis 14-3-3 family of signaling regulators. *Plant Physiol* 2001;126:35–38.
40. Porta H, Rocha-Sosa M. Plant lipoxygenases. Physiological and molecular features. *Plant Physiol* 2002;130:15–21.
41. Christensen SA, Nemchenko A, Borrego E, et al. The maize lipoxygenase, ZmLOX10, mediates green leaf volatile, jasmonate and herbivore-induced plant volatile production for defense against insect attack. *Plant J* 2013;74:59–73.
42. Melan MA, Dong X, Endara ME, Davis KR, Ausubel FM, Peterman TK. An *Arabidopsis thaliana* lipoxygenase gene can be induced by pathogens, abscisic acid, and methyl jasmonate. *Plant Physiol* 1993;101:441–450.
43. Shetty R, Fretté X, Jensen B, et al. Silicon-induced changes in antifungal phenolic acids, flavonoids, and key phenylpropanoid pathway genes during the interaction between miniature roses and the biotrophic pathogen *Podosphaera pannosa. Plant Physiol* 2011;157:2194–2205.
44. Yoshioka H, Yamada N, Doke N. cDNA cloning of sesquiterpene cyclase and squalene synthase, and expression of the genes in potato tuber infected with Phytophthora infestans. *Plant Cell Physiol* 1999;40:993–998.
45. Ma QH, Xu Y. Characterization of a caffeic acid 3-O-methyltransferase from wheat and its function in lignin biosynthesis. *Biochimie* 2008;90:515–524.
46. Vanholme R, Demedts B, Morreel K, Ralph J, Boerjan W. Lignin biosynthesis and structure. *Plant Physiol* 2010;153:895–905.
47. Li K, Xu C, Zhang J. Proteome profile of maize (*Zea Mays* L.) leaf tissue at the flowering stage after long-term adjustment to *rice black-streaked dwarf virus* infection. *Gene* 2011;485:106–113.
48. Tholl D, Chen F, Petri J, Gershenzon J, Pichersky E. Two sesquiterpene synthases are responsible for the complex mixture of sesquiterpenes emitted from arabidopsis flowers. *Plant J* 2005;42:757–771.
49. Eigenbrode SD, Ding H, Shiel P, Berger PH. Volatiles from potato plants infected with potato leafroll virus attract and arrest the virus vector, *Myzus persicae* (Homoptera: Aphididae). *Proc Biol Sci* 2002;269:455–460.
50. Srinivasan R, Hall DG, Cervantes FA, Alvarez JM, Whitworth JL. Strain specificity and simultaneous transmission of closely related strains of a *Potyvirus* by *Myzus persicae. J Econ Entomol* 2012;105:783–791.